Desalination and Water Treatment
www.deswater.com

doi:10.5004/dwt.2016.11378

76 (2017) 40–52
May

Membrane distillation and reverse osmosis based desalination driven by geothermal energy sources

Jamel Orfi[a,*], Abdullah Najib[a], Emad Ali[b], Abdulhamid Ajbar[b], Maher AlMatrafi[c], Mourad Boumaaza[b], Khalid Alhumaizi[b]

[a]*Mechanical Engineering Department, King Saud University, Riyadh, Saudi Arabia, emails: orfij@ksu.edu.sa (J. Orfi), anmohammed@ksu.edu.sa (A. Najib)*
[b]*Chemical Engineering Department, King Saud University, Riyadh, Saudi Arabia, emails: amkamal@ksu.edu.sa (E. Ali), aajbar@ksu.edu.sa (A. Ajbar), mouradb@ksu.edu.sa (M. Boumaaza), humaizi@ksu.edu.sa (K. Alhumaizi)*
[c]*Graduate Student of the Master of Science in Desalination Engineering program, College of Engineering, King Saud University, Riyadh, Saudi Arabia, email: maher@saudieng.org*

Received 13 July 2015; Accepted 17 November 2016

ABSTRACT

Geothermal energy has been widely used in power generation and heating. However, its utilization in water desalination is not common due to several barriers and limitations including the saline water quality to be treated and the high cost of such a combined process. Some brackish desalination plants using reverse osmosis (RO) membranes are constructed and under operation. In some of these plants, the raw water is first cooled by damping its heat into the atmosphere using cooling towers. The cooled brackish water is then pumped to the RO membranes. This work discusses several configurations of using geothermal energy to drive desalination of brackish waters. It focuses on the modeling and simulation of a direct contact membrane distillation (DCMD) unit powered by geothermal energy sources. The performance of the whole system composed of the geothermal energy source and the desalination unit is modeled using balance equations of mass, energy and species. Hybrid desalination linking membrane distillation (MD) and RO units is also investigated. The results illustrate the benefits of combining the MD-RO and geothermal energy source in terms of enhancement of the plant recovery ratio. They show in particular that the overall recovery ratio for low salinity feed solutions (lower than 2,000 ppm) is high. The simulations show that it can be around 79% and 67% when the feed salinity equals 800 and 2,000 ppm, respectively.

Keywords: Geothermal energy; Direct contact membrane distillation; Integrated RO and DCMD; Recovery ratio; Brackish water

1. Introduction

The shortage of potable water in KSA forces the country to develop reliable sea and brackish water desalination technologies with high performance and low cost. Several dual purpose power and desalination and hybrid (thermal/membrane) plants based on conventional technologies are constructed or under construction. Fig. 1 shows the total water demand and planned supply sources curves between 2005 and 2025 in Saudi Arabia [1]. The use of new desalination processes including membrane distillation (MD) driven by renewable energy sources such as solar and geothermal becomes attractive. This is reflected by the increasing number of studies on such integrations [2,3]. MD can be used single or integrated with other processes such as reverse osmosis (RO) process.

*Corresponding author.

Presented at EuroMed 2015: Desalination for Clean Water and Energy Palermo, Italy, 10–14 May 2015. Organized by the European Desalination Society.

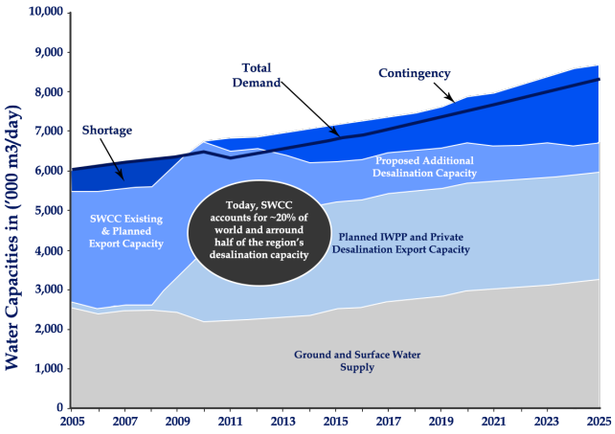

Fig. 1. Saudi total water demand versus planned supply sources (in 1,000 m^3/day, 2005–2025) [1]; SWCC – Saline Water Conversion Corporation; IWPP – Independent Water and Power Producers.

1.1. Geothermal energy in KSA

Geothermal energy utilization includes electric power generation and several direct applications. Lund et al. [4] reviewed the worldwide applications of geothermal energy for direct utilization including bathing and swimming, space and district heating and ground source heat pumps. Specific data and information up to 2015 on geothermal utilization for about 82 countries were gathered, presented and discussed. They reported that the installed thermal power for direct utilization at the end of 2014 is around 71,000 MWt. The geothermal energy use in Saudi Arabia consists of an installed capacity of 40 MWt for bathing and swimming and 4 MWt for animal farming for total direct use applications of 152.89 TJ/year [4].

The available data and information on geothermal resources in KSA are few and somehow contradictory in some cases. In fact, the number of hot wells and their maximum temperatures are not well defined. Several studies identified ten thermal springs: six in Jizan (southwest near the Yemen border) and four in Al-Lith area (west-central on the Red Sea). Seventeen surface water occurrences were also recognized. Al Dayel [5] reported that the temperature levels measured are ranging from 70°C to 100°C. Rehman and Shash [6] reported that there are several hot springs with varying deep temperature of 50°C–120°C and different flow rates. Table 1 gives the physical properties of thermal springs. It is shown that for the cited locations, the temperature level is lesser than 80°C.

Taleb [7] discussed the barriers hindering the utilization of geothermal resources in Saudi Arabia. She noted that despite the availability of some potentially rich-geothermal locations, KSA has not undertaken any serious geothermal projects. Taleb [8] divided the barriers to two subgroups, namely technical and non-technical (political, economic, social and educational). The main economic barrier is the availability of a subsidized cheap source of energy (fossil fuels). This barrier is identified also for the case of other renewable energy sources such as solar energy.

Recently, AlHarbi [9] conducted a survey on the available geothermal energy resources in the country. He classified them based on exergy using a Specific Exergy Index (SEI). He divided the country in five departments (central, northern, western, eastern and southern) with eight regions. Table 2 gives some important characteristics of the available geothermal resources including the temperature, the salinity, the flow rate and the depth. The SEI values for all the identified geothermal wells are found very low meaning that they are of a very low grade energy. Therefore, their potential use is limited to low enthalpy applications including heating, low temperature desalination such as low temperature multiple effect distillation (LT-MED), humidification and dehumidification (HDH) and MD.

Table 1
Some physical properties of thermal springs in KSA (adapted from Rehman and Shash [6])

Name	Temperature, °C	Flow rate (L/min)
Ain Khulab (Gizan)	75.5	1–2
Wadi Khulas (Gizan)	31.4	10
Ain Khulan Quwa (Gizen)	59	2
Ain al Wagrah (Gizan)	55	1.5
Ain al Wagrah Dam (Gizan)	59	20
Ain al Harra (Al Lith)	79	4–5
Ain ak Jumah (Al Lith)	46	0.3
Ain Markus (Al Lith)	46	0.3
Ain al Darakah (Al Lith)	39.5	0.1

Recent studies on geothermal energy resources and potentials in KSA are encouraging. Chandrasekharam [10] reported that Saudi power potential can reach 5 GW. Source temperatures of 95°C or higher have been reported [11,12]. Lashin and AlArifi [11] focused on the potential of geothermal energy in the southern region of Saudi Arabia and its utilization in power generation. The work aimed mainly to explore and locate the potentiality of these resources through analyzing the available satellite images and performing a geophysical survey, as well as estimating the geothermal reserve potential for possible energy production. The specific site of Wadi Al-Lith is considered one of the most promising geothermal targets with many hot springs with a surface temperature up to 95°C (Hussain et al. [12]). Recent data in Rubu Alkhali with surface temperature of 97°C, total dissolved salts (TDS) of 4,127 ppm, flow rate of 454.2 m^3/h have been reported [9].

On the other side, based on King Abdullah City for Atomic and Renewable Energy (Ka-care) studies, the use of geothermal energy is expected to be important in the next decades. For instance, the renewable energy targets for KSA by 2032 are planned as follows: 50% of electricity from non-hydrocarbon resources: 54 GW from renewables (of which: 41 GW from photovoltaic (PV) and concentrated solar power (CSP), 9 GW wind, 3 GW waste-to-energy, 1 GW geothermal) and 17.6 GW from nuclear [13].

The geothermal energy utilization in water desalination is not common due to several barriers and limitations including the saline water quality to be treated and the high cost of such a combined process. Some desalination plants using RO membranes are constructed and under operation such as those near Riyadh city [14–16]. In some of these plants, the geothermal energy contained in the feed water is

Table 2
Summary of the main geothermal energy resources in KSA [9]

Region	Department	Longitude	Latitude	Range of temperature (°C)	Range of TDS (ppm)	Range of flow rate (m^3/day)	Range of depth (m)
Riyadh	Central	–	–	34–70	500–1,000	3792–8640	1,800–2,000
Asir	Southern	–	–	15–26	155–1,630	20–1500	11–350
Gizan	South	–	–	31.4–75.5	1,500–2,500	2.16–28.8	25–30
Medina	Western	39.733	24.183	31–41	300–600	6750–8500	75–262
Tabuk	Western	36.097	29.126	27	350–500	5,400	550
Al-Lith	Western	–	–	39.5–79	2,500–3,000	0.144–6.48	25–40
Hail	Northern	42.029	27.983	27	500–700	4,300–5,600	350
Arar	Northern	40.899	30.965	48	500	13,300	1,450

first damped into the atmosphere using cooling towers. The cooled brackish water is then pumped to the RO membranes. Thus, cooling towers are used in the pretreatment section to cool the feed water before entering the RO units [14,15]. A recent study focused on the operational performance of a RO plant in Howtat Bani Tamim city located at 190 km south of Riyadh. The TDS concentrations of the feed water and the permeate water are 2,000 and 29 ppm, respectively. The overall recovery ratio approaches 87.7%. The pretreatment of the raw water includes evaporative cooling using cooling towers [15]. For Manfouha RO plants which started in 1985 with a total production of 57,600 m^3/d, the raw water pumped from deep wells is cooled to a temperature lower than 35°C [16].

1.2. Membrane distillation

MD is a relatively new and promising membrane technology, which can be used for several applications including desalination. Unlike other membrane technologies, where the driving force is the total fluid pressure, the driving force in MD is the difference in water vapor pressure across a hydrophobic membrane through which only the generated vapor can pass. The formed vapor is condensed in a second step using one of several methods. These methods differ by how the vapor pressure difference across the membrane is imposed and how the formed vapor is condensed. Four main configurations namely direct contact membrane distillation (DCMD), air gap membrane distillation (AGMD), vacuum membrane distillation (VMD) and sweeping gas membrane distillation (SGMD) are usually used and investigated [17–19]. The DCMD configuration is the most common and used in a wide range of applications. This configuration is easy to set up, has lower energy consumption and produces high flux of water permeate [17]. MD process has several major benefits namely its simplicity, the low level of operating temperature and pressure and its low energy consumption. Moreover, since the process operates at liquid–vapor equilibrium, a total rejection of macromolecules ions and other non-volatile components can be obtained [20]. This high rejection rate and the high quality of the permeate observed by different authors are almost independent on the feed water salinity. Recently, Safavi and Mohammadi [20], for instance, conducted an experimental analysis on desalination using VMD of high salinity water with concentrations ranging from 100 to 300 g/L.

Besides, another major advantage of the MD process is that the feed water can be heated by any cheap energy source (i.e., solar, geothermal or waste energy from diesel engines or from cogeneration plants). The use of solar energy to drive MD units has been considered by several authors [21–23]. The integration of geothermal energy to drive desalination units is, on the other hand, not widely used compared to solar energy, even if both are considered as low grade energies.

On the other side, the use of MD technology is still limited. This fact is due to several factors including numerous problems related to the membrane properties mainly its hydrophobicity, the low production rates, low recovery ratio and fouling and scaling [17–19]. It is important to mention that recently published works have investigated the MD performance enhancement using various arrangements and configurations including the incorporation of a heat recovery device integrated with the MD system [24,25] and the use of multi-stage (or multi effect) concept [25,26]. The latter is well known and is commonly used in multiple effect distillation and multi-stage flash technologies. Its use in MD would increase the recovery ratio as well as reduce the specific energy consumption of the process.

1.3. Geothermal energy and desalination

In a recent work, Davies and Orfi [27] noticed that the use of geothermal energy specifically for desalination is a relatively unexplored topic with only a few studies conducted. They proposed a framework study showing the technical feasibility of self-powered geothermal desalination of groundwater sources at ≤100°C. Thus, desalination can be matched with geothermal energy using different methods. For example, Multi Flash Distillation (MSF) can be coupled with medium temperature geothermal energy. RO unit can be driven by geothermal power plant. Li et al. [28] reported several advantages of using geothermal energy for desalination. In addition to the low environmental impacts, stability and reliability of the geothermal energy, the authors noticed that typical geothermal source temperatures ranging from 70°C–90°C are suitable for low temperature multiple effect distillation (MED) technology.

Several studies have been conducted to investigate the performance of geothermal sources coupled with desalination units. Examples of these studies are those of Bourouni et al. [29], Mohamed and El Minshawy [30]

and Mahmoudi et al. [31] (HDH process), Koroneos and Roumbas [32] (MED process), Loulatidou and Arafat [33] (MED and RO), Bouchekima [34] (solar stills), Bouguecha and Dhabi [35] (MD process). Sarbatly and Chiam [36] evaluated the energy utilization of VMD modules corresponding to three types of lab-fabricated membranes and one commercial membrane. The main properties including the porosity, the thickness and the gas permeability were obtained and their respective effects on process performance were studied. The use of geothermal energy source was investigated technically and economically. The results show in particular that the geothermal energy can save about 95% of the total energy consumption.

The use of MD integrated with other processes particularly RO has been the subject of some recent studies. Mericq et al. [37] proposed an integrated VMD-RO unit where the VMD was considered as complimentary process to the RO to further concentrate the RO discharged brines and then increase the overall recovery of the plant. El-Zanati and El-Khatib [38] proposed a hybrid system consisting of nanofiltration (NF) and RO followed by VMD. The overall recovery for sea water was increased from 30–35% to 76.2%, respectively when using RO and the hybrid system. Pangarkar et al. [39] reviewed the coupling of RO and MD processes for desalination of groundwater. They gave several advantages of using such integrated systems for the groundwater water in India. Zhang et al. [40] analyzed various factors affecting the thermal efficiency of MD process including the use of heat recovery techniques. Ji et al. [41] conducted an investigation on the performance of a MD crystallization unit operated on brines from a sea-water RO unit. A water recovery ratio of 90% was obtained.

In the following sections, a theoretical model for the heat and mass transfer for DCMD configuration is presented and used for a parametric study. The model is used also to investigate the performance of a multi-stage DCMD unit. The last part of the work concerns the integration of MD and RO units using geothermal energy sources.

2. DCMD model

2.1. Heat and mass transfer model

The transport phenomena in MD process are described and analyzed in different studies. Several simplifications and assumptions on the heat and mass transfers have been the basis of various theoretical models [42,43]. The heat transfer mechanism in DCMD process can be explained using the schematic diagram shown in Fig. 2.

The temperature gradient between the hot feed and cold permeate resulting in a partial water vapor pressure difference on the membrane sides drives the generated vapor through the microporous membrane. Therefore, the vapor mass flux can be described as:

$$J = C_m(P_{v1} - P_{v2}) \tag{1}$$

where P_{v1} and P_{v2} are the vapor pressures at the hot and cold sides of the membrane, respectively.

The partial pressure for pure water vapor as function of temperature can be calculated using the Antoine equation [44]:

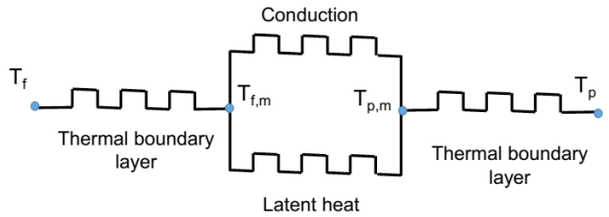

Fig. 2. Heat transfer resistances in MD process.

$$P_w = \exp\left(23.1964 - \frac{3816.44}{T_i - 46.13}\right) \tag{2}$$

where T_i refers to membrane surface temperature.

For non-ideal binary mixtures, the partial pressure should take into account the effect of salinity:

$$P_i = \chi_w a_w P_w \tag{3}$$

where χ_w is the liquid mole fraction of water and a_w is the water activity [44]:

$$a_w = 1 - 0.5\chi_{NaCl} - 10\chi^2_{NaCl} \tag{4}$$

where χ_{Nacl} refers to the mole fraction of NaCl in the solution.

C_m in Eq. (1), the overall mass transfer coefficient, is usually expressed in terms of three transport mechanisms namely molecular diffusion, Knudsen diffusion and viscous flow. The nature of the dominant diffusion mechanism is governed by the Knudsen number defined as:

$$kn = \frac{\lambda}{d} \tag{5}$$

where d, a characteristic length, is the mean pore diameter of the membrane and λ is the mean free path of water molecules, expressed as [45]:

$$\lambda = \frac{k_B T}{\sqrt{2}\pi P d_e^2} \tag{6}$$

where k_B, T and P refer to the Boltzmann constant, absolute temperature and average pressure inside the membrane pores, respectively, while d_e is the collision diameter of the water vapor and air. The mean path value of water vapor at 60°C is estimated to be 0.11 µm [46].

For small Knudsen numbers (lower than 0.01), molecular diffusion is the dominant mechanism while when kn is high (higher than 1), Knudsen diffusion is the dominant. For intermediate values ($0.01 < kn < 1$), both phenomena are important and should be superposed. Table 3 gives the expressions of these diffusion models.

Regarding the heat transfer mechanism in DCMD, it can be described as [44,45] (see Fig. 2):

- Convective heat transfer in the feed boundary layer,
- Combined conduction heat transfer through the membrane and latent heat associated with vapor generation within the membrane,
- Convective heat transfer in the permeate boundary layer.

Table 3
Expressions of Knudsen diffusion, molecular diffusion and Knudsen-molecular transition models [45,47]

Mass flux	Knudsen diffusion	Molecular diffusion	Knudsen/molecular transition
$J = C_m\left(P_{v1} - P_{v2}\right)$	$C_m^k = \frac{2\varepsilon r}{3\tau\delta}\left(\frac{8M}{\pi RT}\right)^{1/2}$	$C_m^D = \frac{\varepsilon}{\tau\delta}\frac{PD}{P_a}\frac{M}{RT}$	$C_m^C = \left[\frac{3}{2}\frac{\tau\delta}{\varepsilon\delta}\left(\frac{\pi RT}{8M}\right)^{1/2} + \frac{\tau\delta}{\varepsilon}\frac{P_a}{PD}\frac{RT}{M}\right]^{-1}$

Table 4
Expressions of heat rates in the feed, membrane and permeate regions

Heat transfer	Feed side	Membrane	Cold side
Expression	$q_f = h_f\left(T_f - T_1\right)$	$q_m = JH_v + k_m\frac{dT}{dx}$	$q_c = h_c\left(T_2 - T_c\right)$

Table 4 summarizes the rates of heat transfer in the feed, membrane and permeate regions. At steady state, the DCMD process overall heat flux q_t can be expressed as:

$$q_f = q_m = q_c = q_t = U(T_f - T_c) \tag{7}$$

The overall heat transfer coefficient U may be given as:

$$U = \left[\frac{1}{h_f} + \frac{1}{\frac{k_m}{\delta_m} + \frac{JH_v}{T_1 - T_2}} + \frac{1}{h_c}\right]^{-1} \tag{8}$$

The effective thermal conductivity k_m can be estimated from the gas and solid phase thermal conductivities k_g and k_s, respectively, and the membrane porosity ε as:

$$k_m = (1-\varepsilon)k_s + \varepsilon k_g \tag{9}$$

Using the above equations, the membrane surface temperatures T_1 and T_2 can be obtained:

$$T_1 = \frac{\frac{k_m}{\delta_m}\left(T_c + \frac{h_f}{h_c}T_f\right) + h_f T_f - JH_v}{\frac{k_m}{\delta_m} + h_f\left(1 + \frac{k_m}{\delta_m h_c}\right)} \tag{10a}$$

$$T_2 = \frac{\frac{k_m}{\delta_m}\left(T_f + \frac{h_c}{h_f}T_c\right) + h_c T_c + JH_v}{\frac{k_m}{\delta_m} + h_c\left(1 + \frac{k_m}{\delta_m h_f}\right)} \tag{10b}$$

The ratio of the actual driving force to the maximum driving force is defined as the temperature polarization coefficient (TPC):

$$\mathrm{TPC} = \frac{T_1 - T_2}{T_f - T_c} \tag{11}$$

Similarly, a concentration boundary layer adjacent to the membrane surface is associated with the concentration polarization coefficient CPC:

$$\mathrm{CPC} = \frac{C_w}{C_f} \tag{12}$$

where C_w and C_f are the wall (membrane) and feed bulk concentrations, respectively.

The surface concentration C_w can be estimated using the film theory as [44,48]:

$$C_w = C_f \exp\left(\frac{J}{\rho h_m}\right) \tag{13}$$

where J is the mass flux and h_m is the mass transfer coefficient. The latter can be evaluated using the heat and mass transfer analogy [44].

The heat transfer coefficient h_t is calculated using an appropriate correlation among several ones [22,44,45]. In this work, Graetz-Leveque correlation which is recommended for laminar flow is used [44]:

$$Nu = 1.86\left(\mathrm{ReP}\gamma\frac{d_h}{L}\right)^{0.33} \tag{14}$$

where d_h, the hydraulic diameter is defined as $d_h = \frac{4A_c}{P_e}$.

The thermal efficiency of the process is expressed as:

$$\mathrm{EE} = \frac{JH_v A_e}{Q_t} * 100 \tag{15}$$

where J is the formed vapor flux, H_v refers to the latent heat of vaporization. A_e is the membrane area and Q_t is the total energy supplied to the feed water.

2.2. MD model and validation

The above governing equations describing the heat and mass transfer in a single stage DCMD module were solved as a system of equations using Engineering Equations Solver (EES) [49]. EES, a widely used solver for thermo-fluids applications uses a Newton iteration method to solve non-linear set of equations [50]. The thermo-physical properties of saline water were evaluated using appropriate correlations implemented in EES. The results obtained

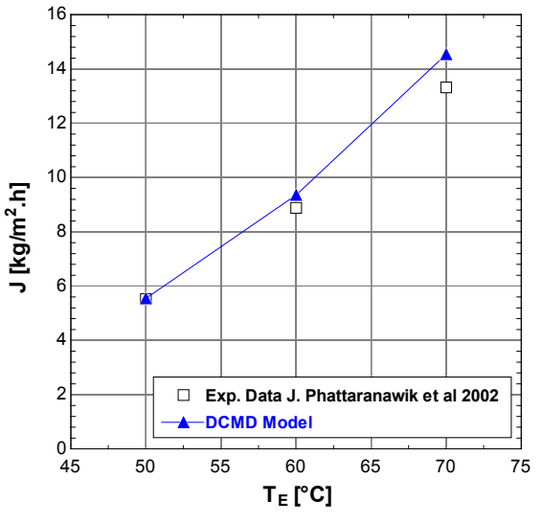

Fig. 3. The computed mass flux (J) for different inlet feed temperatures (T_F) and comparison with the experimental results of Phattaranawik et al. [42].

by the present model were evaluated using available information from literature. In particular, the present model outputs have been compared with the numerical results of Nakoa et al. [47]. Excellent agreements have been obtained. Besides, the experimental results of Phattaranawik et al. [42] were used for further validation of the model. Fig. 3 shows the variation of the water mass flux with the applied inlet feed temperature as evaluated by the present model and obtained experimentally by Phattaranawik et al. [42]. As a general comment, one can notice a fair agreement between the results of the present model and those of [42].

3. Results and discussion

The present study can be divided into two sections. The first one focuses on a parametric analysis for DCMD module. The second section deals with integrated MD and RO units.

3.1. MD results

The calculations were made for a DCMD module with basic parameters given in Table 5. The membrane has an area of 0.0572 m², thickness of 45 µm, length of 26 cm and a hydraulic diameter d_h of 4 mm. Liquid circulation rates on the hot and cold sides are 0.075 and 0.1136 m/s, respectively. The corresponding Reynolds numbers are 594.3 and 432.35 indicating laminar flows.

Fig. 4 shows schematically a basic configuration for a single MD stage composed of several flat sheet membrane modules. Each module is a simple counter flow DCMD system with no energy recovery. It consists of hot and cold streams separated by a membrane.

The effect of temperature difference between feed and permeate sides ($T_f - T_c$) on the formed vapor mass flux, process efficiency, temperature polarization coefficient are reported in Figs. 5–7. Fig. 5 displays the effect of ($T_f - T_c$) on the vapor mass flux for four values of feed salinity. It shows that as ($T_f - T_c$) increases from 20°C to 60°C,

Table 5
Fixed parameters referring to the DCMD module used in the simulations

Parameters	Hot flow	Permeate (cold) flow
Geometry information		
Hydraulic diameter (d_h) (mm)	4	4
Effective area (m²)	0.0572	
Thickness of membrane (m)	45×10^{-6}	
Length of membrane (m)	0.260	
Operation conditions		
Inlet velocity (V) (m/sec)	0.075	0.1136364
Volume flow rate ($Q = \pi/4 * d_h^2 * V$)	9.425×10^{-7} (m³/sec)	1.428×10^{-6} (m³/sec)
	0.05655 (L/min)	0.0857 (L/min)
Temperature (T) (°C)	70	20
Salinity (Sal) (ppm)	37,000	0
Reynolds number (–)	594.30	432.35
Prandtl number (–)	3.19	7.34
Nusselt number (–)	5.66	6.71
Schmidt number (–)	504.80	-
Sherwood number (–)	30.11	-
Membrane properties		
Porosity	0.85	
Tortuosity	1.176	

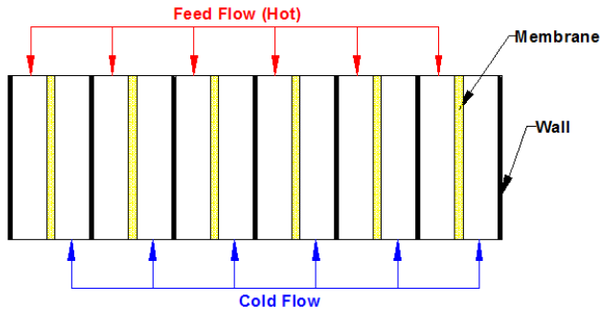

Fig. 4. Compartments for one stage.

the vapor flux goes up from about 1 to about 7 kg/h/m². Such a trend of exponential behavior may be attributed to the temperature-vapor pressure relation given by Antoine's equation. Fig. 5 shows also that permeate flux from sea water is slightly lower than that from brackish water (salinity lower than 10,000 ppm). Such a reduction in the mass flux due to the feed salinity can be explained by the additional boundary layer that would be formed on the membrane surface. This concentration boundary layer combined with the thermal boundary layer would reduce the driving force of the process. It can be noticed that for concentrations lower than 10,000 ppm, permeate flux can be considered as independent on the feed salinity.

The process thermal efficiency known also as evaporation efficiency is defined as the ratio between the useful heat

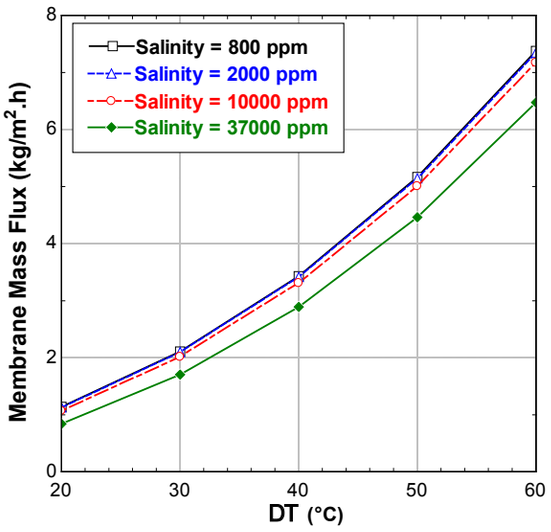

Fig. 5. Effect of the temperature difference between feed and permeate streams on the vapor mass flux for various feed salinity values.

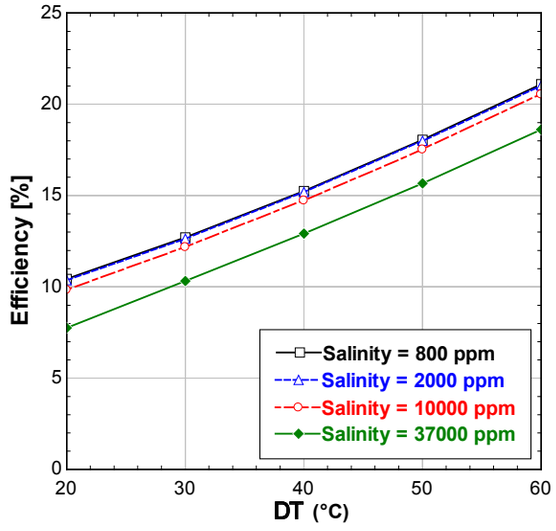

Fig. 6. Effect of the temperature difference between feed and permeate streams and the feed salinity on the DCMD thermal efficiency.

and the total added heat. It is plotted as function of $(T_f - T_c)$ and feed salinity in Fig. 6. Summers and Lienhard [50] used the gain output ratio (GOR), commonly employed in conventional thermal desalination technologies, as a measure of thermal performance of the MD process. This indicator can vary from one for single effect distillation or a solar still to more than 15 for MED or MSF with several effects or stages [51]. Dispersed values of GOR ranging from 0.17 to 4.1 are reported for single stage MD. Nakoa et al. [47] suggested that for more adequacy the GOR should include not only the supplied thermal energy but also the pumping electrical energy.

Fig. 6 shows a linear behavior of the thermal efficiency with the feed to the permeate temperature difference. For sea

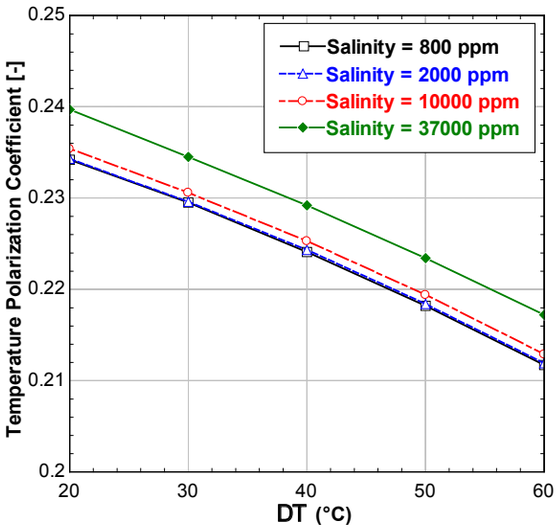

Fig. 7. Effect of the temperature difference between feed and permeate streams and the feed salinity on the temperature polarization coefficient.

water, the evaporation efficiency is lower than the case of the brackish water. In overall, only between 10% and 20% of the total available heat is used showing that DCMD configuration has limited performance. This is mainly due to the heat loss by conduction through the membrane. Similar results on the behavior of thermal efficiency are reported in Nakoa et al. [47].

The theoretical driving force for the MD system is the feed to the permeate difference $(T_f - T_c)$. This assumes that the membrane surface temperatures are equal to the bulk temperatures. In practice, thermal boundary layers on the hot and cold sides of the membrane take place resulting in thermal and mass resistances that would limit the permeate mass flux significantly. Fig. 7 illustrates how the temperature polarization factor (TPC) changes with $(T_f - T_c)$ and with feed salinity. It shows in fact that increasing $(T_f - T_c)$ from 20°C to 60°C reduces the TPC from 23.5% to 21.5% indicating that the actual driving force decreases. This fact might be attributed to the increase of the evaporation rates at higher $(T_f - T_c)$ resulting in a higher mass and thermal resistances. It is of interest to mention here that the obtained values of TPC ranging from 21% to 24% are low meaning the limitations of the DCMD process. In order to increase the TPC, several ideas have been proposed and some of them were implemented and tested [18,45,52]. For example, Lovineh et al. [52] suggested using membranes with low thermal conductivity such as Polypropylene (PP). The inclusion of turbulence promoters and spacers in the flow channels and the use of ultrasonic systems were proposed [17,53,54].

The membrane properties such as the thickness, the thermal conductivity, the porosity and the permeability are very important to have high vapor fluxes and MD performance. Qtaishat and Banat [22] observed that to obtain a high MD permeability, the membrane surface layer should be as thin as possible with large porosity and large pore size. Pore size values ranging from 0.2 to 1 μm have been reported in several MD studies [20]. Fig. 8 illustrates the effect of increasing the membrane porosity from 0.55 to 0.95 on the mass flux. As shown,

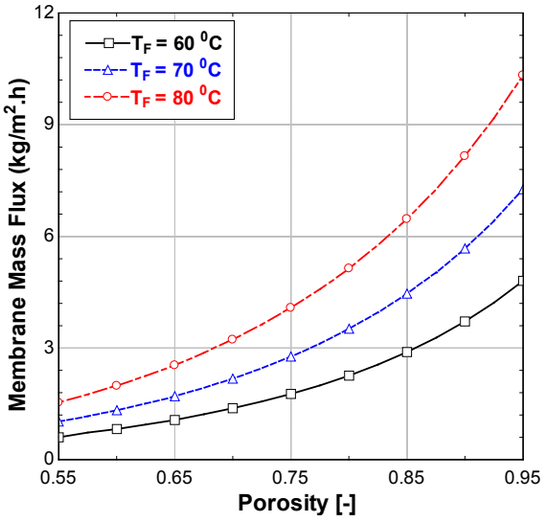

Fig. 8. Variation of the vapor mass flux with the membrane porosity for three feed temperatures.

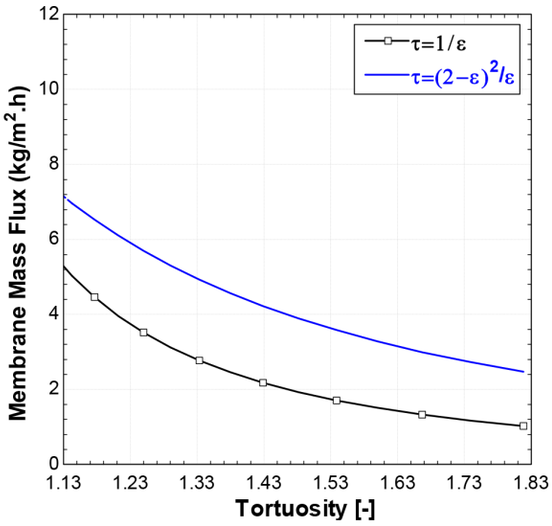

Fig. 9. Variation of the vapor mass flux with the membrane tortuosity using two different expressions.

the vapor mass flux J, exhibits an exponential rise with the porosity especially for high ε and higher feed temperatures. For example J goes up from about 1.8 to more than 10 kg/m²/h when the porosity increases from 0.55 to 0.95. In fact, as ε increases, the available surface area for evaporation rises too and the heat conduction losses decrease since air entrapped in the membrane pores has lower thermal conductivity than the membrane. It is of interest to mention that Lovineh et al. [52] have shown similar trends for J with ε for vacuum MD. Such results have, however, linear behavior rather than the exponential trend observed in the present work.

Another important property affecting the membrane permeability is the tortuosity factor. As this factor goes high the permeability decreases since the diffusing molecules path is tortuous and larger than the membrane thickness. This factor is used to correct such a fact, i.e., the molecules path through the membrane is larger than the membrane thickness [52]. Rao et al. [55] who investigated the characteristics of the membrane properties reported values for the MD tortuosity ranging from 1 to more than 7.

Two widely employed empirical relations expressing the tortuosity as function of the porosity are [18,55,56]:

$$\tau = \frac{1}{\varepsilon} \tag{16a}$$

$$\tau = \frac{(2-\varepsilon)\text{^}2}{\varepsilon} \tag{16b}$$

Rao et al. [55] used the first relation (Eq. (16a)) for the non-woven support of the composite membrane and the second relation (Eq. (16b)) for single layer and active layers of the composite materials. They justified that single layer membranes and active layers of composite materials are spongy while non-woven support layers are loosely packed.

Figs. 9 and 10 illustrate the effect of the tortuosity factor on the permeate mass flux and the concentration polarization coefficient. A similar behavior is observed for the variation of the process thermal efficiency and temperature polarization coefficient. The mass flux of the formed vapor decreases as τ increases. However, for high values of τ (higher than 1.5) its effect becomes weak. On the other side, one can see that using the first relation (Eq. (16a)) gives lower performance.

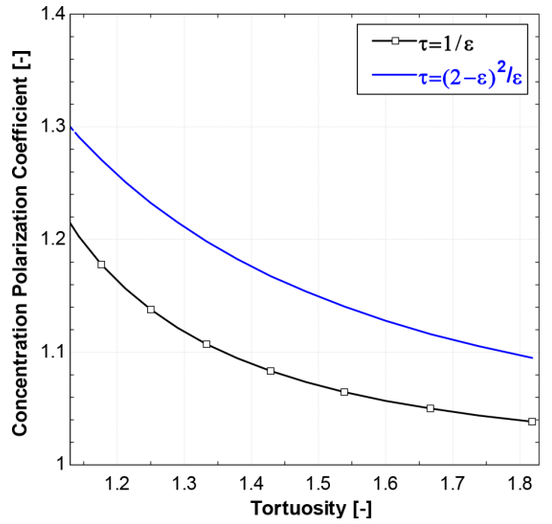

Fig. 10. Variation of the concentration polarization factor with the membrane tortuosity using two different models.

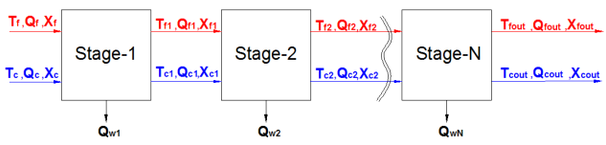

Fig. 11. Schematic diagram of DCMD consecutive stages.

Fig. 11 illustrates the concept of several stages placed in series and in co-current configuration. The hot feed water

with T_f, Q_f and X_f enters the first stage and leaves at lower temperature T_{f1}, lower flow rate Q_{f1} and higher salinity X_{f1}. It enters the second stage with the same properties T_{f1}, Q_{f1} and X_{f1} and so on. On the other side, the cold stream with T_c, Q_c and X_c enters the first stage and leaves at higher temperature T_{c1}, same flow rate Q_{c1} and same salinity X_{c1}.

Fig. 12 illustrates the distribution of the temperatures of the feed, cold, feed-membrane surface and cold-membrane surface within a multi-stage configuration. It shows as the number of stages increases the difference between the hot and cold flow temperatures decreases as expected for the co-current flow configuration. The feed temperature decreases as result of the heat exchange with the membrane for 70°C at the first stage to about 45°C at the end of the unit (Stage 5). The difference between the hot and cold sides of the membrane which is the actual driving force of the process becomes very small at higher stages. This is due to the rapid decrease of the membrane hot side temperature while the cold side temperature remains almost constant. With higher initial feed temperatures, higher number of stages can be obtained.

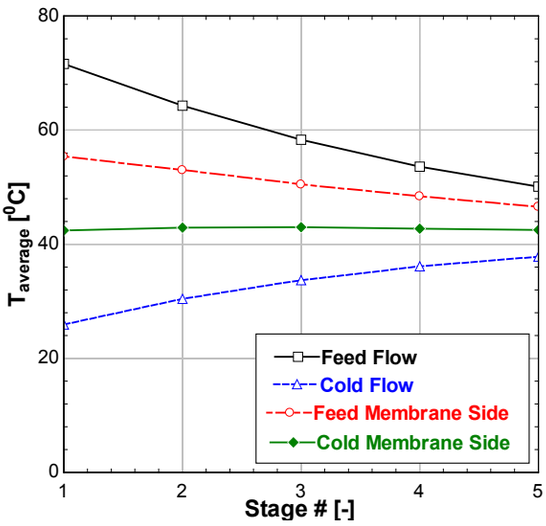

Fig. 12. Temperature distribution of the feed, cold and feed-membrane and cold-membrane surfaces in a multi-stage configuration.

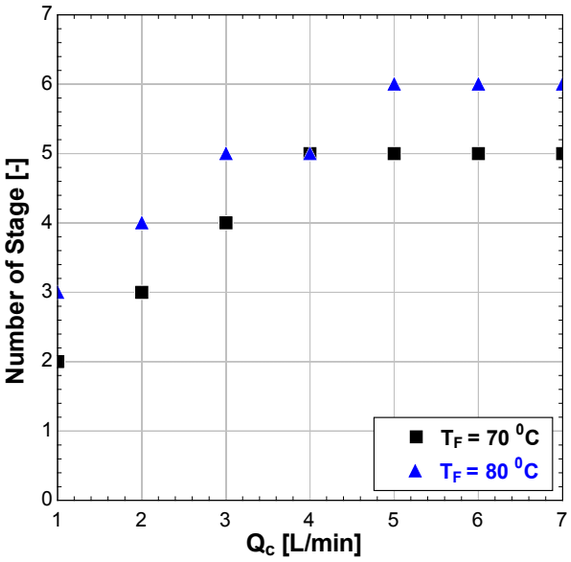

Fig. 13. Effect of the cold flow rate on the size of each DCMD unit.

Fig. 13 illustrates the important effect of the cold flow rate Q_c on the size of each unit. Increasing the stages number leads to an increase of the unit size. This can be obtained by rising Q_c to 5 L/mn for both cases of initial feed temperature of 70°C and 80°C. Fig. 14 shows that in order to reduce

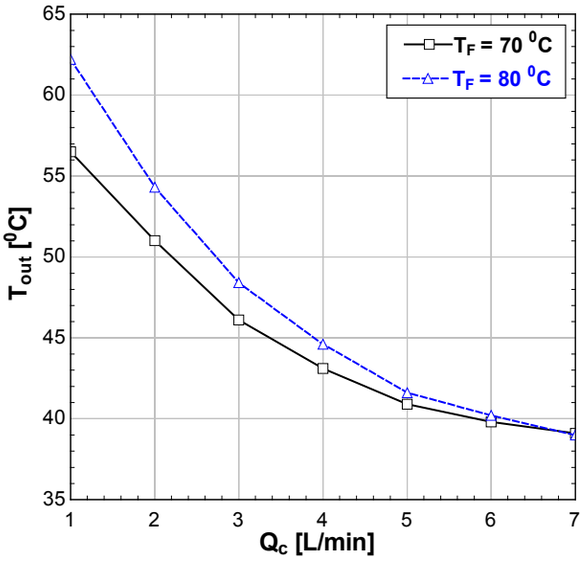

Fig. 14. Effect of the cold flow rate on the outlet feed temperature of the DCMD unit.

Table 6
Effect of feed salinity at temperature of 70°C on the MD unit recovery ratio and concentration factor

Salinity (ppm)	Optimum number of stages	Brine outlet salinity (ppm)	Total recovery (%)	Concentration factor
800	5	1,077	28.75	1.404
2,000	5	2,688	28.62	1.401
10,000	5	13,220	27.05	1.371
37,000	5	46,191	14.35	1.168

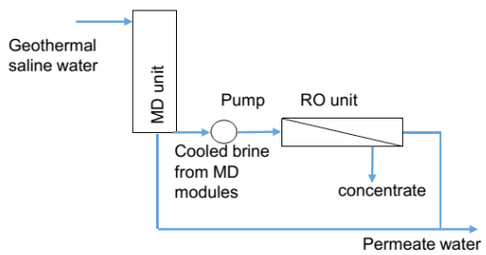

Fig. 15. A schematic for an integrated MD and RO units using geothermal source.

Table 7
Effect of temperature on the recovery and comparison with previous experimental (measured) and theoretical (calculated) values

Temperature (°C)	Recovery			Error (%)	
	Measured values [58]	Calculated values [58]	ROSA Software	Between measured and ROSA values	Between calculated and ROSA values
19	0.64	0.588	0.5324	16.81	9.46
20	0.65	0.595	0.5517	15.12	7.28
21	0.66	0.601	0.5713	13.44	4.94
22	0.66	0.612	0.5912	10.42	3.40
23	0.67	0.613	0.6114	8.75	0.26
24	0.68	0.624	0.6318	7.09	1.25
25	0.68	0.631	0.6524	4.06	3.39
26	0.7	0.651	0.6739	3.73	3.52
27	0.71	0.655	0.6935	2.32	5.88
28	0.72	0.667	0.717	0.42	7.50
29	0.74	0.679	0.7387	0.18	8.79
30	0.75	0.697	0.7604	1.39	9.10
31	0.76	0.707	0.7819	2.88	10.59
32	0.77	0.724	0.8035	4.35	10.98
33	0.78	0.737	0.8245	5.71	11.87
34	0.79	0.748	0.8458	7.06	13.07

the feed outlet temperature of the unit, the cold flow rate should be increased. The effect of the initial feed temperature becomes small when increasing Q_c. On the other side, after stage 5 the increase of Q_c results in a weak reduction in the feed solution temperature.

Table 6 summarizes the effect of the feed salinity on the unit performance for $T_f = 70$°C. For brackish waters with salinity lower than 10,000 ppm, the unit recovery ratio is about 28% while the concentration factor is kept at about 1.37–1.40 showing no significant influence of the feed quality. For high salinity waters, the recovery ratio falls to about 14.3%.

3.2. Integration of MD and RO with geothermal energy

In the following section, the case of desalting hot geothermal waters with temperature of 70°C is investigated using integrated MD and RO units. Fig. 15 shows schematically such an integration. Therefore, the energy of the geothermal water is not damped to the ambient air as in the existing RO plants; it is used to drive the MD unit. This fact is the main reason behind considering this option of coupling RO and MD. It is worthy to mention that the proposed option is not unique. Other options can also be proposed and investigated.

Several simulations showing the influence of feed salinity on the overall system performance were conducted using the developed MD model described in the first part of this work and ROSA software [57] for RO calculations.

Table 8
Operating conditions

Parameters	Value
TDS (ppm)	850
Volume flow rate (m^3/d)	10
PH	8.34
Feed water pressure (bar)	11

Table 9
Specification of the RO element (filter)

LC HR-4040	
Maximum pressure (bar)	15.5
Volume flow rate (m^3/d)	10.98
Rejection (%)	99.5

Table 7 compares the recovery ratio for temperatures ranging from 19°C to 34°C as obtained by the present ROSA simulations to previous theoretical and experimental results of Suleiman et al. [58]. Satisfactory agreements between ROSA results and experimental ones for temperature values between 25°C and 32°C are obtained. The input parameters used to perform these comparisons are given in Tables 8 and 9.

Table 10
Feed salinity effect on the performance of the integrated MD and RO unit (feed temperature 70°C)

Membrane distillation (DCMD)					Reverse osmosis (RO)					Overall system	
Feed salinity (ppm)	Feed temp. T_f (°C)	Brine outlet (ppm)	R_MD (%)	CF_MD	Salinity inlet (ppm)	T_f (°C)	Brine Outlet (ppm)	R_{RO} (%)	CF_{RO}	Recovery R_{total} (%)	CF_{total}
800	70	1,123	28.75	1.404	1,123	34	3,820	70.71	3.402	79.13	4.775
2,000		2,802	28.62	1.401	2,802		6,065	53.93	2.165	67.12	3.033
10,000		13,708	27.05	1.371	13,708		14,557	5.86	1.062	31.32	1.456
37,000		43,199	14.35	1.168	43,199		43,320	0.28	1.003	14.59	1.171

R_MD: Recovery ratio for membrane distillation unit; R_RO: Recovery ratio for reverse osmosis unit; R_Total: Total recovery for both of membrane distillation and reverse osmosis units
CF_MD: Concentration factor for membrane distillation unit; CF_RO: Concentration factor for reverse osmosis unit; CF_Total: Total concentration factor for both of membrane distillation and reverse osmosis units

Table 11
product concentration of the MD - RO integrated unit as function of the feed salinity (feed temperature 70°C)

Feed salinity (ppm)	Xp_{MD} (ppm)	Xp_{RO} (ppm)	Xp_{TOTAL} (ppm)
800	0	5.838	3.717
2,000	0	14.528	8.333
10,000	0	69.73	9.516
37,000	0	138.2	2.272

Table 10 summarizes the main results for an integrated geothermal desalination plant with a DCMD unit followed by RO unit. The temperature of the geothermal water falls in the MD unit from 70°C to 34°C which is appropriate temperature for RO membranes [58]. The RO recovery ratio is very sensitive to the feed salinity at its entry. It falls from 70.71% to 5.86% to 0.28% when the inlet salinity increases from 1,123 to 13,708 to 43,199 ppm, respectively. Adding a MD unit to the RO one enhances significantly the overall performance of the integrated plant. The overall recovery ratio varies from 79% to 31.32% to 14.56% when the initial feed salinity changes from 800, to 10,000 to 37,000 ppm. It is of interest to note that the overall heat recovery ratio for low salinity feed waters (lower than 2,000) is high (higher than 67%). On the other side, using RO unit for seawaters seems not beneficial since no significant amount of freshwater would be added.

Table 11 shows the product concentration as function of the initial feed salinity. For each case, the final product maintains very low salinity.

4. Conclusion

This work deals with desalination using MD and RO driven by geothermal energy. It gives first a review on the states of the geothermal energy in Saudi Arabia and presents the main previous works that have investigated the integration of MD and RO. Theoretical models for the heat and mass transfer with a DCMD module and multi-stage DCMD unit have been developed and validated. The effects of the cold water mass flow rate and the entering feed temperature on the unit size and outlet feed temperature are studied. The corresponding results for MD show in particular that for brackish waters with lower salinity than 10,000 ppm, the unit recovery ratio is about 28% while the concentration factor is about 1.37 with no significant influence of the feed quality. For high salinity solutions, the recovery ratio falls to about 14%. The results on the integration of MD with RO show that the overall recovery ratio for low salinity feed solutions (lower than 2,000 ppm) is high. Other works on this subject are under analysis.

Acknowledgment

This study was funded by the National Plan for Science, Technology and Innovation (MAARIFAH), King Abdulaziz City for Science and Technology, Kingdom of Saudi Arabia (12-WAT2616-02).

References

[1] A. Al-Arifi, Desalination in the Kingdom of Saudi Arabia, Saline Water Conversion Corporation SWCC, KSA, June 17, 2013. Available at: www.slideplayer.com/slide/3410215/.
[2] N. Ghaffour, J. Bundschuh, H. Mahmoudi, M.F.A. Goosen, Renewable energy driven desalination technologies: a comprehensive review on challenges and potential applications of integrated systems, Desalination, 356 (2015) 94–114.
[3] V.G. Gude, Energy storage for desalination processes powered by renewable energy and waste heat sources, Applied Energy, 37 (2015) 877–898.
[4] J.W. Lund, T.L. Boyd, Direct utilization of geothermal energy 2015 worldwide review, Geothermics, 60 (2016) 66–93.

[5] M. Al Dayel, Geothermal Resources in Saudi Arabia, Geothermics, 17 No. 2/3, 1988, pp. 465–476.
[6] S. Rehman, A. Shash, Geothermal Resources of Saudi Arabia – Country Update Report, Proceedings World Geothermal Congress 2005, Antalya, Turkey, April 2005, pp. 24–29.
[7] H.M. Taleb, An Investigation into the Barriers Impeding the Development of Geothermal Potential in Saudi Arabia, International Conference and Exhibition on Green Energy & Sustainability for Arid Regions & Mediterranean Countries, Amman, Jordan, November 2009, pp. 10–12.
[8] H.M. Taleb, Barriers hindering the utilization of geothermal resources in Saudi Arabia, Energy Sustain. Dev., 13 (2009) 183–188.
[9] M. Alharbi, Geothermal Energy in Saudi Arabia and Its Application in Desalination, Master's Thesis, Department of Mechanical Engineering, King Saud University, KSA, 2014, p. 90.
[10] D. Chandrasekharam (Personal Information), Visiting Professor, King Saud University, 2012.
[11] A. Lashin, N. Al Arifi, Geothermal energy potential of southwestern of Saudi Arabia – exploration and possible power generation: a case study at AlKhouba area – Jizan, Renew. Sustainable Energy Rev., 30 (2014) 771–789.
[12] M.T. Hussein, A. Lashin, A. Al Bassam, N. Al Arifi, I. Al Zahrani, Geothermal power potential at the western coastal part of Saudi Arabia, Renew. Sustainable Energy Rev., 26 (2013) 668–684.
[13] B. Hashem, Geothermal Development Roadmap for the Kingdom of Saudi Arabia, King Abdullah City for Atomic and Renewable Energy, Saudi Arabia. Available at: http://www.oit.edu/docs/default-source/geoheat-center-documents/quarterly-bulletin/vol-31/312/31-2-art6.pdf?sfvrsn=4.
[14] Available at: http://www.wabag.com/wabag-projects/al-wasia-desalination-plant, accessed on 19 September 2016.
[15] K.H. Khalil, F.M. Wali, A.M. El-Dosari, Operational performance and monitoring of a reverse osmosis desalination plant: a case study, IJCET, 5 (2015) 3760–3767.
[16] I.S. A1-Mutaz, B.A. Al-Sultan, Prediction performance of RO desalination plants, Desalination, 120 (1998) 153–160.
[17] M.S. El-Bourawi, Z. Ding, R. Ma, M.A. Khayat, Framework for better understanding membrane distillation separation process, J. Membr. Sci., 285 (2006) 4–29.
[18] M.I. Ali, E.K. Summers, H.A. Arafat, J.H. Lienhard V, Effects of membrane properties on water production cost in small scale membrane distillation systems, Desalination, 306 (2012) 60–71.
19] I. Hitsov, T. Maere, K. De Sitter, C. Dotremont, I. Nopens, Modelling approaches in membrane distillation: a critical review, Sep. Purif. Technol., 142 (2015) 48–64.
[20] M. Safavi, T. Mohammadi, High-salinity water desalination using VMD, Chem. Eng. J., 149 (2009) 191–195.
[21] H.E.S. Fath, S.M. Elsherbiny, A.A. Hassan, M. Rommel, M. Wieghaus, J. Koschikowski, M. Vatansever, PV and thermally driven small-scale, stand-alone solar desalination systems with very low maintenance needs, Desalination, 225 (2008) 58–69.
[22] M.R. Qtaishat, F. Banat, Desalination by solar powered membrane distillation systems, Desalination, 308 (2013) 186–197.
[23] J. Koschikowski, M. Wieghaus, M. Rommel, V. Subiela Ortin, V. Peñate Suarez, J.R.B. Rodríguez, Experimental investigations on solar driven stand-alone membrane distillation systems for remote areas, Desalination, 248 (2009) 125–131.
[24] G. Guan, X. Yang, R. Wang, A.G. Fane, Evaluation of heat utilization in membrane distillation desalination system integrated with heat recovery, Desalination, 366 (2015) 80–93.
[25] E. Drioli, A. Ali, F. Macedonio, Membrane distillation: recent developments and perspectives, Desalination, 356 (2015) 56–84.
[26] H. Geng, J. Wang, C. Zhang, P. Li, H. Chang, High water recovery of RO brine using multi-stage air gap membrane distillation, Desalination, 355 (2015) 178–185.
[27] P. Davies, J. Orfi, Self-powered desalination of geothermal saline groundwater: technical feasibility, Water, 6 (2014) 3409–3432. doi:10.3390/w6113409.
[28] C. Li, Y. Goswami, E. Stefanakos, Solar assisted sea water desalination: a review, Renew. Sustainable Energy Rev., 19 (2013) 136–163.
[29] K. Bourouni, J.C. Deronzier, L. Tadrist, Experimentation and modelling of an innovative geothermal desalination unit, Desalination, 125 (1999) 147–153.
[30] A. Mohamed, N. El Minshawy, Humidification–dehumidification desalination system driven by geothermal energy, Desalination, 249 (2009) 602–608.
[31] H. Mahmoudi, N. Spahis, M. Goosen, S. Sablani, S. Abdul-Wahab, N. Ghaffour, N. Drouiche, Assessment of wind energy to power solar brackish water greenhouse desalination units: a case study from Algeria, Renew. Sustainable Energy Rev., 13 (2009) 2149–2155.
[32] C. Koroneos, G. Roumbas, Geothermal waters heat integration from the desalination of sea water, Desal. Wat. Treat., 37 (2012) 69–76.
[33] S. Loulatidou, H.A. Arafat, Techno-economic analysis of MED and RO desalination powered by low-enthalpy geothermal energy, Desalination, 365 (2015) 277–292.
[34] B. Bouchekima, A small solar desalination plant for the production of drinking water in remote arid areas of southern Algeria, Desalination, 159 (2003) 197–204.
[35] S. Bouguecha, M. Dhahbi, Fluidised bed crystalliser and air gap membrane distillation as a solution to geothermal water desalination, Desalination, 152 (2003) 237–244.
[36] R. Sarbatly, C.K. Chiam, Evaluation of geothermal energy in desalination by vacuum membrane distillation, Applied Energy, 112 (2013) 737–746.
[37] J.P. Merciq, S. Laborie, C. Cabassud, Vacuum membrane distillation of seawater reverse osmosis brines, Water Res., 44 (2010) 5260–5273.
[38] E. El-Zanati, K.M. El-Khatib, Integrated membrane based desalination system, Desalination, 205 (2007) 15–25.
[39] B.L. Pangarkar, M.G. Sane, M. Guddad, Reverse osmosis and membrane distillation for desalination in groundwater: a review, ISRN Mater Sci., 1–9 (2011) Article ID 523124.
[40] Y. Zhang, Y. Peng, S. Ji, Z. Li, P. Chen, Review of thermal efficiency and heat recycling in membrane distillation processes, Desalination, 367 (2015) 223–239.
[41] X. Ji, E. Curcio, S. Al Obaidani, G. Di Profio, E. Fontananova, E. Drioli, Membrane distillation crystallization of seawater reverse osmosis brines, Sep. Purif. Technol., 71 (2010) 76–82.
[42] J. Phattaranawik, R. Jiraratananon, A.G. Fane, Effects of net-type spacers on heat and mass transfer in direct contact membrane distillation and comparison with ultrafiltration studies, J. Membr. Sci., 217 (2003) 193–206.
[43] T.C. Chen, C.D. Ho, H.M. Yeh, Theoretical modeling and experimental analysis of direct contact membrane distillation, J. Membr. Sci., 330 (2009) 279–287.
[44] Ó. Andrjesdóttir, C.L. Ong, M. Nabavi, S. Paredes, A.S.G. Khalil, B. Michel, D. Poulikakos, An experimentally optimized model for heat and mass transfer in direct contact membrane distillation, Int. J. Heat Mass Transfer, 66 (2013) 855–867.
[45] A. Alkhudiri, N. Darwish, N. Hilal, Membrane distillation: a comprehensive review, Desalination, 287 (2012) 2–18.
[46] S. Al-Obaidani, E. Curcio, F. Macedonio, G. Di Profio, H. Al-Hinai, E. Drioli, Potential of membrane distillation in seawater desalination: thermal efficiency, sensitivity study and cost estimation, J. Membr. Sci., 323 (2008) 85–98.
[47] K. Nakoa, A. Date, A. Akbarzadeh, A research on water desalination using membrane distillation, Desal. Water Treat., 56(10) (2015) 2618–2630.
[48] A. Bahmanyar, M. Asghari, N. Khoobi, Numerical simulation and theoretical study on simultaneously effects of operating parameters in direct contact membrane distillation, Chem. Eng. Process.: Process Intens., 61 (2012) 42–50.
[49] S.A. Klein, Engineering Equation Solver (EES), Academic Commercial Version 9.725, F-chart; 2014. Available at: http://www.fchart.com/ees/
[50] E. Summers, J.H. Lienhard V, Experimental study of thermal performance in air gap membrane distillation systems, including the direct solar heating of membranes, Desalination, 330 (2013) 100–111.

[51] H.T. El-Dessoukey, H.M. Ettouney, Fundamentals of Salt Water Desalination, 2002, Elsevier, ISBN 0-444 5081-04.
[52] S. Lovineh, M. Asghari, B. Rajaei, Numerical simulation and theoretical study on simultaneous effects of operating parameters in vacuum membrane distillation, Desalination, 314 (2013) 59–66.
[53] L. Martínez-Díez, M.I. Vázquez-González, F.J. Florido-Díaz, Study of membrane distillation using channel spacers, J. Membr. Sci., 144 (1998) 45–56.
[54] C. Zhu, G.L. Liu, C.S. Cheung, C.W. Leung, Z.C. Zhu, Ultrasonic stimulation on enhancement of air gap membrane distillation, J. Membr. Sci., 161 (1999) 85–93.
[55] G. Rao, S.R. Hiibel, A.E. Childress, Simplified flux prediction in direct-contact membrane distillation using a membrane structural parameter, Desalination, 351 (2014) 151–162.
[56] S.B. Iversen, V.K. Bhatia, K. Dam-Johansen, G. Jonsson, Characterization of micro porous membranes for use in membrane contactors, J. Membr. Sci., 130 (1997) 205–217.
[57] ROSA Software. Available at: http://www.dow.com/, accessed on 20 May 2016.
[58] S. Suleiman, A. Meree, M. AL-Shiakh, F. Kroma, Performance of RO plant with solar preheated feed water, Desal. Wat. Treat., 28 (2011) 345–352.